Geometry and spatio-temporal evolution of the 2001 Agios Ioanis earthquake swarm (Corinth Rift, Greece)

Francesco Pacchiani, Hélène Lyon-Caen

Geophys. J. Int. (2010) **180,** 59–72 doi: 10.1111/j.1365-246X.2009.04409.x

Geometry and spatio-temporal evolution of the 2001 Agios Ioanis earthquake swarm (Corinth Rift, Greece)

Francesco Pacchiani* and Hélène Lyon-Caen

Laboratoire de Géologie, Ecole Normale Supérieure, CNRS 24 *rue Lhomond,* 75231 *Paris cedex* 05, *France. E-mail: fpacchiani@inogs.it*

Accepted 2009 October 2. Received 2009 July 28; in original form 2008 March 3

SUMMARY

The Agios Ioanis earthquake swarm occurred below the southern edge of the Corinth Rift (Greece). The swarm is of interest due to its location and especially because the activated structure is oriented at a high angle to the rift's major active normal faults. We present a detailed study of the swarm including a high-resolution relocation of multiplets, accompanied by an analysis of their geometry and of their spatio-temporal evolution. *P*- and *S*-wave traveltime delays, calculated in the spectral domain to within subsampling precision, are inverted considering all pairs of events. In a second step, the large-scale structure of the swarm is refined by inverting traveltime delays calculated from absolute wave arrival-times. The relocation image, in combination with the results of the multiplet geometrical analysis, reveals a complex structure suggesting seismic activity on parallel planes that strike southwest and dip to the northwest. We propose that this fault zone connects to the Kerinitis Valley, where geological observations suggest the presence of a transverse fault linking normal faults striking 100°N. The spatio-temporal evolution of the relocated seismicity provides evidence of a $\sim$20 m day^{-1} migration of seismic activity towards the surface. Assuming fluid-driven seismicity, we model the spatio-temporal evolution as the diffusion of a pore-pressure perturbation. The preferred model indicates a hydraulic diffusivity equal to 0.1 m^2 s^{-1}, suggesting that the spatio-temporal evolution of the seismicity is related to fluid flow at depth. Moreover, we estimate the hydraulic conductivity (1.15×10^{-5} m s^{-1}) and the rock permeability (7×10^{-13} m^2), which compare well to available local observations.

Key words: Permeability and porosity; Plasticity, diffusion, and creep; Earthquake source observations; Seismicity and tectonics; Continental tectonics: extensional; Dynamics and mechanics of faulting.

1 INTRODUCTION

The spatial distribution of microseismicity is very important in deciphering complex fault structures at depth. In general, images obtained by earthquake location are not precise enough to allow more than a large-scale geometrical description of the active fault zone. Indeed, routine hypocentre calculations involve uncertainties of kilometre scale depending on network geometry. To improve hypocentre locations, earthquake relocation methods were developed (e.g. Poupinet *et al.* 1984; Console & Di Giovambattista 1987), which significantly decrease the location error and deliver high-resolution images of active structures (e.g. Got *et al.* 1994; Waldhauser & Ellsworth 2000).

Analysis of relocated seismicity enables to retrieve the geometry at depth of the active faults. The precision of the geometrical description depends on the accuracy of earthquake locations, thus high-resolution earthquake relocation is crucial. Adding information on the temporal distribution of earthquakes allows, moreover, to recover the spatio-temporal evolution of seismicity and to study fault mechanics. Owing to increasing quantities of acquired data and to the decrease in the magnitude of completeness of seismic catalogs, evidence of natural earthquake migration in spatio-temporal seismicity patterns is augmenting (e.g. Chiaraluce *et al.* 2004; Miller *et al.* 2004; Jenatton *et al.* 2007; Bourouis & Cornet 2009). This phenomenon is mostly observed in studies of earthquake swarms and seems related to fluid circulation at depth (Noir *et al.* 1997; Miller *et al.* 2004; Antonioli *et al.* 2005) in a similar way to hydraulically induced earthquakes that migrate coherently with the propagation of induced pore-pressure perturbations (Shapiro *et al.* 1997; Phillips *et al.* 2002; Hainzl 2004). However, considering natural seismicity, it is difficult to establish the presence and involvement of fluids, and it is especially hard to quantify their state and the changes they induce in a fault zone.

In this paper, we present a high-resolution analysis of an earthquake swarm, recorded in the framework of the European Corinth Rift Laboratory project, which occurred in the western Corinth Rift,

*Now at: Istituto Nazionale di Oceanografia e di Geofisica Sperimentale Borgo Grotta Gigante 42/C, 34010 Sgonico (TS), Italy.

Greece. After a brief description of the tectonics and the seismicity of the region, we present the 2001 Agios Ioanis earthquake swarm and explain the methods employed for its relocation and geometrical analysis. We then present the high-resoution relocation results and discuss the influence of the network configuration. Thereafter, the geometry and spatio-temporal evolution of the swarm are described followed by a discussion on the hypothesis of a fluid-driven earthquake swarm and its implications for rock physical properties.

2 TECTONIC SETTING

The Corinth Rift, located between the Peloponnese and northern Greece (Fig. 1), is currently the most active of numerous normal fault systems located in the northern Aegean. It is part of a deforming area between the western termination of the North Anatolian Fault in the northern Aegean Sea, the subducting African plate and the Kephallonia Fault in the Ionian Sea (e.g. McKenzie 1972). The rift is 110 km long and extends, in an E–W direction, from the Corinth Canal to the Gulf of Patras. Geological observations suggest an asymmetric half graben (e.g. Brooks & Ferentinos 1984; Armijo *et al.* 1996) and focal mechanisms of $M > 5.5$ historical earthquakes (e.g. King *et al.* 1985; Rigo *et al.* 1996; Bernard *et al.* 1997) as well as GPS observations of the past 15 years (e.g. Briole *et al.* 2000; Avallone *et al.* 2004) indicate N–S extension. The deformation rate across the rift is 3 mm yr^{-1} in the east and increases westwards, culminating at 16 mm yr^{-1} near the city of Aigion. Analysis of the GPS data suggests that the deformation is concentrated along a narrow WNW-ESE band, 10 km wide, situated in the centre of the rift, under the Gulf of Corinth (Briole *et al.* 2000; Avallone *et al.* 2004). This implies a very high strain rate, consistent with the very high seismicity rate observed in the Aigion area (Lyon-Caen *et al.* 2004).

The rift's major normal faults strike WNW-ESE and are predominantly located on the southern coast of the gulf (Fig. 1). They are composed of segments, 15–20 km long, organized *en échelon*, that dip to the north at 50–70° (e.g. Armijo *et al.* 1996; Micarelli *et al.* 2003). Active offshore synthetic and antithetic faults, steeply dipping at angles of 60–70°, have also been identified (e.g. Moretti *et al.* 2003). In the western part of the rift, bordering the southern coast of the gulf, the West Helike Fault is probably the oldest active fault (Bernard *et al.* 2006).

3 THE AGIOS IOANIS EARTHQUAKE SWARM

The permanent Corinth Rift Laboratory network (CRLNET) (Lyon-Caen *et al.* 2004) covers a 30 × 30 km study area around the city of Aigion (Figs 1 and 2) and started recording in June 2000. It is composed of 12, short-period ($f_0 = 2$ Hz), three component seismometers. Half are located on the southern coast of the gulf in boreholes 60–130 m deep. In addition, we used stations DAFN, LAKA (both operated by the University of Athens) and SERG (jointly operated by Patras University and Charles University, Prague) equipped with broad-band seismometers. All stations sample at 125 Hz, except SERG that samples at 100 Hz.

During the year 2001, 6604 events were located by CRLNET using HYPO71 software (Lee & Lahr 1972) and the 1-D velocity model and V_p/V_s ratio (1.80) determined by Rigo *et al.* (1996). The 2147 best located events (Fig. 2) have uncertainties in epicentral location of 0.5 km and in depth of 1 km. Other events have, on average,

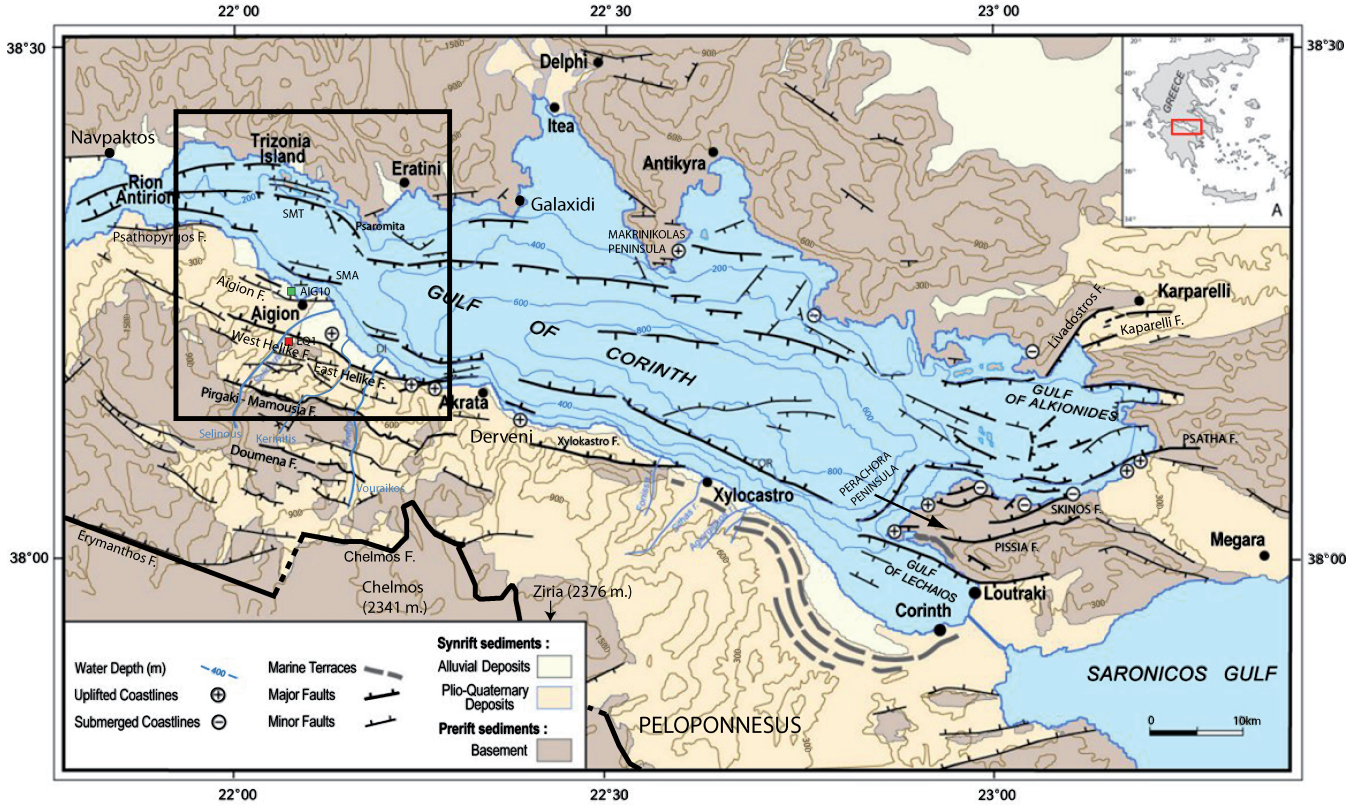

Figure 1. Tectonic map of the Corinth Rift. The box delimits the study area around the city of Aigion. The green square represents the location of the AIG10 borehole (Cornet *et al.* 2004) and the red square that of the EQ1 well (Giurgea *et al.* 2004). Modified after Moretti *et al.* (2003).

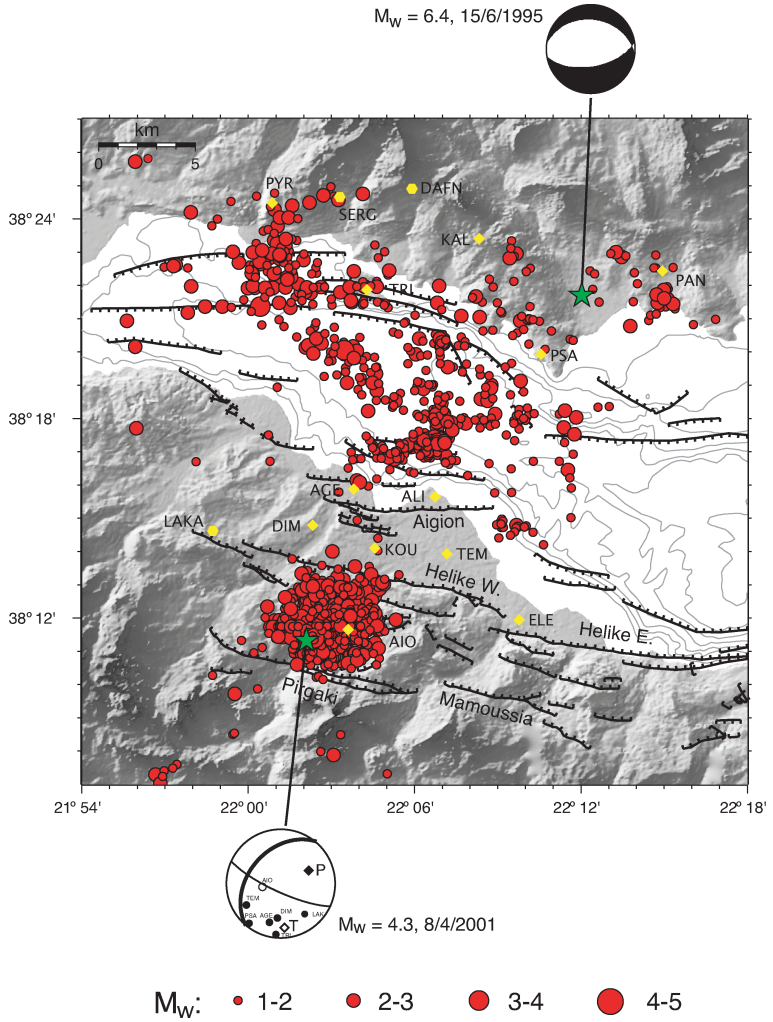

Figure 2. Map of the western Corinth Rift showing epicentres (red circles) of the 2147 best located earthquakes that occurred in year 2001, that is, those with at least five *P*-wave and four *S*-wave readings and with an *RMS* smaller than 0.1 s. Yellow symbols indicate recording stations. The green star to the south indicates the location of the $M_w = 4.3$ Agios Ioanis earthquake of April 8, 2001 and the one to the north indicates the location of the $M_w = 6.4$ Aigion earthquake of June 15, 1995. Focal mechanisms are from Zahradník *et al.* (2004) for the former earthquake and from Bernard *et al.* (1997) for the latter.

uncertainties twice as large. The magnitude of the events varies between $M_w = 0.5$–4.3 and the catalog is complete from $M_w = 1.4$ (Pacchiani 2006). The main characteristics of this seismicity are: (1) a seismogenic layer situated between 4 and 15 km depth, (2) a thin band of seismicity under the gulf, gently dipping to the north between 7 and 10 km depth, whose detailed structure is still under study (Lambotte *et al.* 2007) and (3) earthquake clustering in space and time (Fig. 2 in Lyon-Caen *et al.* 2004).

The easily recognizable Agios Ioanis earthquake sequence is located on the southern coast, between the surface traces of the Pirgaki and West Helike Faults (Fig. 2). The former fault is geologically inactive since at least 250 ka (Flotté 2003) and the latter is considered to generate only low seismic activity (Bernard *et al.* 2006). This unusual sequence began on March 28, 2001 and involved more than 2900 events over a period of 100 days. The largest event, the $M_w = 4.3$ Agios Ioanis earthquake, occurred on April 8, 2001. The focal mechanism of this earthquake (Fig. 2, Zahradník *et al.* 2004) indicates normal faulting with a strong component of strike-slip motion. Based on the spatial distribution of the mapped seismicity, the nodal plane dipping to the NW (220°N/40°N), indicating an oblique dextral slip, is assumed to be the active fault plane (Lyon-Caen *et al.* 2004). Despite a significantly different fault orientation than that of the major active normal faults of the rift, the T axis of the focal mechanism is consistent with regional N–S extension.

A detailed analysis of the data suggests that the Agios Ioanis sequence developed as a swarm rather than as a mainshock–aftershock sequence. The term swarm, in this study, will be used in a broad sense to mean an earthquake sequence that significantly departs from the definition of a standard mainshock–aftershock sequence (Scholz 2002). The cumulative earthquake distribution shows two major phases of elevated seismicity rate (49 and 31 earthquakes/day on average) separated by 40 days during which the average rate decreases to a lower value of 16 earthquakes/day (Fig. 3a). The last peak of activity is actually split into two peaks of similar rate separated by only 6 days, an unusual feature for an aftershock sequence (Fig. 3b). To fit the decay of seismic activity after the first peak (day 98) with an Omori law ($1/t^p$), an exponent $p < 0.5$ is necessary, and after the last peak of activity an exponent $p = 0.7$ is needed to explain the data. These exponents are low for an aftershock sequence (Fig. 3b), for which they normally range between 0.9 and 1 (Scholz 2002), which is significantly higher than the apparent background rate of about 2 events/day (measured between days 236 and 365).

The earthquake magnitude evolution also corroborates the hypothesis of a swarm. The sequence starts with a $M_w = 3.5$ event

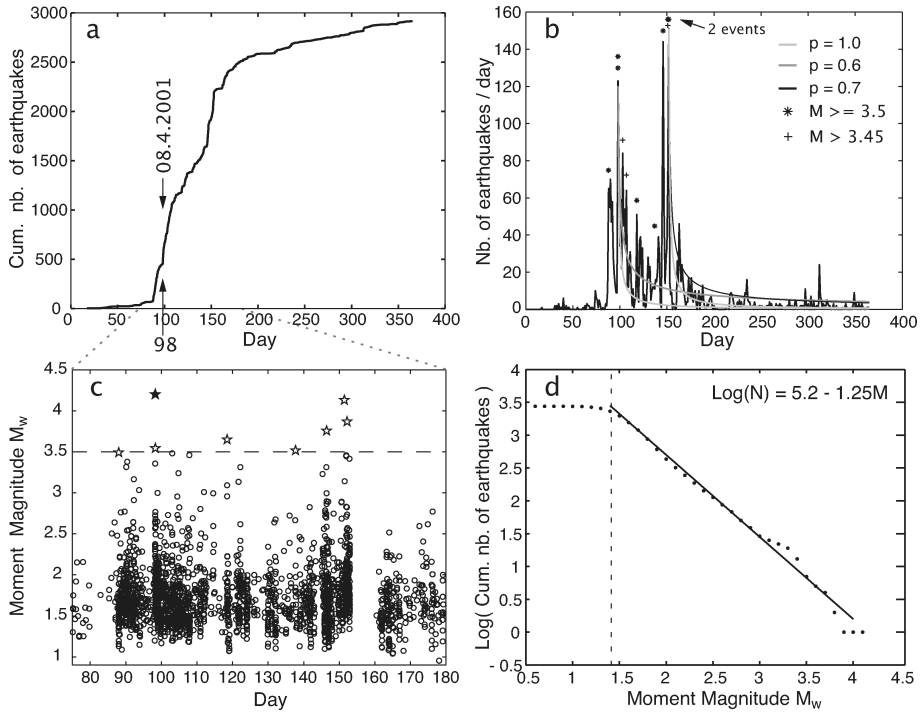

Figure 3. (a) Cumulative number of earthquakes as a function of time for the events of the 2001 Agios Ioanis earthquake sequence. The arrows indicate the $M_w = 4.3$ Agios Ioanis earthquake. (b) Seismicity rate as a function of time. Gray curves follow the Omori law, $R = 1/t^p$, where the exponent p is varied. (c) Moment magnitude as a function of earthquake origin time. Empty stars represent the earthquakes of magnitude $M_w \geq 3.5$ and the solid star represents the Agios Ioanis earthquake. The absence of earthquakes between days 154–158 corresponds to a gap in the available data. (d) Frequency-size distribution of the 2001 earthquake sequence events showing a b-value equal to 1.25. The vertical dotted line indicates the magnitude of completeness of the catalog, $M_w = 1.4$.

followed, 10 days later, by a peak of activity during which the $M_w = 4.3$ Agios Ioanis earthquake occurred. Only 24 minutes later, a second $M_w = 3.5$ earthquake occurred. Four of the eight largest earthquakes ($M_w \geq 3.5$) cluster at the end of the sequence, three of which ($M_w = 3.8$–4.1) occur within the last two peaks of high activity (Fig. 3c). This temporal evolution of the magnitude does not decrease with time as expected in an aftershock sequence (Scholz 2002). Moreover, the seismicity that accompanies the largest earthquakes is greater in terms of number of events for the two peaks at the end of the sequence than for the one at the beginning and related to the Agios Ioanis earthquake. The b-value for the sequence is 1.25 (Fig. 3d). High b-values are thought to be associated with heterogeneous material and low effective normal stresses, a setting that is thought to favor the occurrence of earthquake swarms (Scholz 2002).

4 RELOCATION METHOD

We relocated the swarm earthquakes with the aim of obtaining a high-resolution image of the seismicity and of the active faults at depth. Of interest to us is, first of all, a highly accurate image of the individual multiplets (groups of earthquakes with similar waveforms) and secondly a precise image of the overall swarm. The high accuracy is important because we need a maximum of reliable fault plane orientations from a large number of small multiplets. To achieve this, we adopted a two-step procedure that involved, on the one hand, relocating earthquakes of each multiplet using the technique developed by Got *et al.* (1994) and, on the other hand, relocating multiplets using HypoDD (Waldhauser & Ellsworth 2000). The latter allowed us to improve the accuracy of the multiplets' location and enhance the resolution of the relocation at a larger scale, while the high-precision earthquake relocation allowed us to estimate reliable fault plane parameters from individual multiplets.

Multiplets are extracted from the seismicity before relocating. To this end, for all combinations of earthquake pairs, the seismograms are analysed in the spectral domain and their similarity classified with an equivalence class algorithm (Got *et al.* 1994). This technique is based on the coherency, which quantifies the linear relationship between two signals as a function of frequency.

The relocation technique developed by Got *et al.* (1994), unlike the Master–Slave technique, considers the *P*- and *S*-wave delays (travel-time differences) for all combinations of earthquake pairs, thereby offering a greater number of constraints on the relocation. The delays for earthquake pairs are measured at each station after alignment of the corresponding seismograms, an operation accomplished in the frequency domain by spectral analysis (Oppenheim & Schafer 1975; Poupinet *et al.* 1984). The latter analysis consists in computing the cross-spectrum and measuring, by regression, the slope of the unwrapped phase spectrum, which is equal to the time lag between the same phase of two seismograms (Poupinet *et al.* 1984; Frechet 1985; Got *et al.* 1994). This technique enables the measurement of delays with millisecond precision, therewith to reduce location errors by up to two orders of magnitude (Poupinet *et al.* 1984). Although we obtain very low relative location uncertainties, the absolute location of each multiplet conserves the initial location error of the reference earthquake. The latter is the best located event of each multiplet, the one recorded by the greatest number of stations and with the smallest *RMS*.

By relocating the reference earthquakes, we aim to improve the multiplet locations. This is achieved by computing the delays for all pairs of reference earthquakes, considering the absolute wave

arrival-times, and inverting them using HypoDD, which is set to singular value decomposition mode (Waldhauser & Ellsworth 2000).

The subsequent analysis of the relocated earthquakes consists in estimating the geometry of the individual multiplets. Assuming that the earthquakes of each multiplet are related to the activation of a fault patch, the analysis is reduced to estimating the best fitting plane. For this, we use the 'Three-Point' method (Fehler *et al.* 1987). It consists in calculating, first, the poles of the planes that pass through each combination of three hypocentres and then the pole density for 294 elements of equivalent area that form, following Fryer's scheme (Fryer 1975), the lower hemisphere of a stereographic projection. If the pole density distribution has a clear maximum, it defines the geometry of the multiplet, that is, of its associated plane. In the presence of inconsistent multiple maxima, we ignored the multiplet geometry.

To confirm the geometry, we used additional information from focal mechanisms. The latter were computed for all earthquakes with at least six clear first arrival polarity recordings. As the solution is generally not very well constrained, due to a non-optimal azimuthal station coverage, we forced the strike domain to $\pm 45^{\circ}$ with respect to the value estimated by the Three-Point method. This guarantees that the multiplet geometry is not in contradiction with the first wave-arrival polarities. For each multiplet, a representative focal mechanism is selected and then compared to the result of the Three-Point method. If one of the nodal planes agrees with the plane described by the pole density maximum, the active fault plane is confirmed and considered well constrained. In case of disagreement, the multiplet is rejected.

5 RELOCATION OF THE SWARM

Setting the coherency threshold to 0.85, we extracted 27 multiplets containing at least five earthquakes, involving a total of 1263 earthquakes, equivalent to 43 per cent of the earthquake swarm (2917 events). Seismograms of earthquakes from two multiplets are shown as examples in Fig. 4. Multiplet 1, the largest, is composed of 769 earthquakes that represent 26 per cent of the earthquake swarm, and 15 multiplets contain at least 10 events (Table 1). The predominance of small multiplets is mostly due to the short time interval considered, 100 days, in contrast to other earthquake relocation studies that generally consider years of seismicity (e.g. Got *et al.* 1994; Rubin & Gillard 2000; Schaff *et al.* 2002; Waldhauser & Ellsworth 2002).

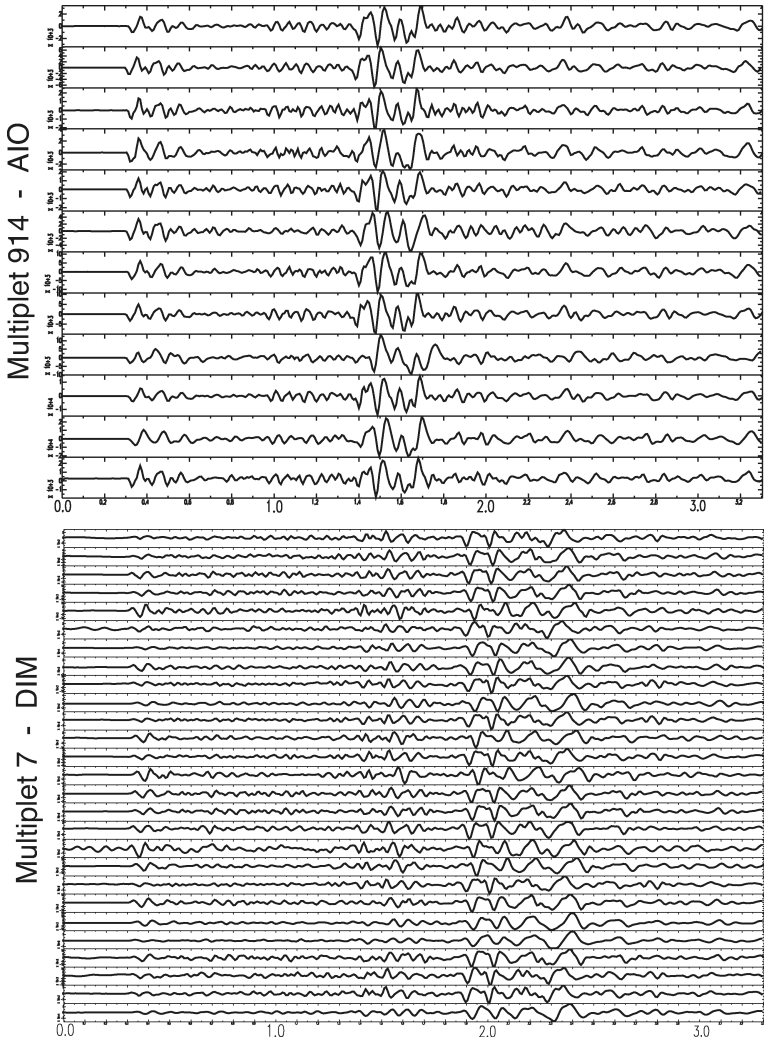

Figure 4. Examples of multiplets extracted from the 2001 Agios Ioanis earthquake sequence. Top panel: waveforms recorded at station AIO for the 12 earthquakes of multiplet 914, extracted using a coherency threshold of 0.9 and bottom panel: waveforms recorded at station DIM for the 27 earthquakes of multiplet 7, extracted using a coherency threshold of 0.85. The horizontal axis represents time in seconds.

The earthquakes of the multiplets are relocated using Got's method (Got *et al.* 1994). Isolated events, whose distance to the other members of a multiplet after relocation is greater than 600 m, as well as those relocated with less than 10 *P*-wave delays were rejected. All except the two largest multiplets (1 and 2) are contained in a volume smaller than 500 × 500 × 500 m (Table 1). For all multiplets, an $RMS \leq 4$ ms was attained after a maximum of three iterations.

The uncertainties in the relocated hypocentres of each multiplet were estimated via 300 Monte-Carlo simulations. In each simulation, the traveltime differences were perturbed with random uniform deviates between ± half the sampling interval (4 ms), which represents the maximum theoretical error on the delays. The resulting error bars on the relative positions are of the order of tens of metres. However, these are lower bound estimates because they only account for the error in the measurement of the delays in the spectral analysis and do not consider errors in the model. Analysis of station residuals gives a more representative global error. In our case, residuals are in general smaller than 10 ms. Thus, assuming a *P*-wave velocity of 5.7 km s^{-1}, the maximum error is approximately 60 m.

In the case of multiplet 1, the residuals are at most 15 ms, so the same reasoning as above leads to a hypocentral error of 90 m. The greater uncertainty is due to the multiplet's larger dimensions (2901 × 2125 m), which induce a greater ray take-off angle error. To check the stability of the result and to gain resolution, this multiplet is subdivided in 23 sub-multiplets (see the 900 series, Table 1), which were extracted with a coherency threshold of 0.9. The submultiplets involve 471 earthquakes, equivalent to 61 per cent of multiplet 1. They are relocated with Got's method (Got *et al.* 1994) and, in addition, the reference earthquakes are relocated using HypoDD. The comparison of the submultiplet relocation with that of the original multiplet 1 shows no significant difference in the large scale (>500 m) aspect of this multiplet. In contrast, there are noticeable differences in the earthquake spatial distribution at a scale of 100–200 m, indicating that the submultiplet relocation is better at resolving finer details.

All reference earthquakes (of multiplets and sub-multiplets) are relocated together with HypoDD and the final result (965 earthquakes, 33 per cent of the swarm) is presented in Fig. 5. Multiplet 1 is not present but is replaced by its submultiplets. The uncertainty in the reference earthquakes' location (in other words, in the multiplets' relative location) is reduced to less than 50 m. The figure clearly demonstrates the significant increase in resolution obtained by earthquake relocation and reveals the detailed structure at depth of the faults activated during the swarm. The earthquakes are aligned on a northwest dipping plane that strikes southwest (Fig. 5, top row, profile b–b'), which is in very good agreement with the focal mechanism of the $M_w = 4.3$ Agios Ioanis earthquake. In the deeper part, a single plane is well defined, whereas at shallower depth (<7 km), the seismic activity is more dispersed and suggests a more complex structure.

Table 1. Table summarizing information on the relocated multiplets and sub-multiplets and their reference earthquakes.

	Number of eqs	Dimensions x (m)	y (m)	z (m)	Reference earthquake Date–Origin time	M_w
Multiplet						
1	769	2901	2126	1617	2001.04.08–16.48.19	1.8
2	122	1508	588	954	2001.03.29–02.04.06	1.9
3	60	434	316	397	2001.06.22–04.42.32	1.8
4	30	313	355	351	2001.03.29–15.33.12	1.6
5	26	173	314	194	2001.04.01–04.39.44	2.0
6	29	296	250	229	2001.03.29–00.42.23	1.4
7	27	477	168	323	2001.03.29–13.41.36	2.4
8	24	260	277	228	2001.05.30–15.47.43	2.1
9	16	437	234	159	2001.06.23–11.39.12	2.1
10	19	449	133	394	2001.11.08–18.49.12	1.7
11	8	61	108	33	2001.05.15–21.50.12	1.5
13	17	552	402	200	2001.04.08–07.34.49	2.8
14	10	57	58	38	2001.04.08–10.23.12	2.0
15	14	104	136	98	2001.06.14–22.06.13	1.9
16	10	322	218	132	2001.03.08–07.52.25	2.1
17	8	77	221	217	2001.05.29–21.34.00	1.6
18	10	241	260	260	2001.04.08–06.23.44	2.4
20	7	94	117	93	2001.05.21–17.40.20	1.7
21	8	182	190	218	2001.03.29–04.52.46	2.0
22	8	51	63	40	2001.04.14–22.39.44	2.2
23	8	106	247	158	2001.05.01–16.12.18	1.5
25	7	112	316	191	2001.05.29–08.27.39	2.1
26	4	39	60	36	2001.05.22–01.15.11	2.2
30	5	58	90	116	2001.04.08–13.30.30	2.0
34	4	205	177	20	2001.06.24–23.16.39	1.6
44	5	37	113	106	2001.05.10–23.46.55	1.5
45	8	204	127	405	2001.07.14–05.46.19	2.7
Submultiplet						
901	91	1032	566	614	2001.04.01–11.08.46	2.1
902	66	534	371	226	2001.04.13–01.27.39	1.9
904	34	360	330	392	2001.04.01–13.23.15	1.7
905	26	251	251	120	2001.04.02–23.11.31	2.0
906	27	238	351	75	2001.05.26–17.56.02	1.4
907	29	521	311	244	2001.04.02–16.49.00	2.0
908	18	274	148	145	2001.04.04–21.24.48	1.8
910	19	82	167	125	2001.03.29–18.44.19	1.6
911	16	204	256	147	2001.04.19–18.46.39	1.8
912	14	72	175	104	2001.04.11–07.45.16	1.8
914	12	239	67	98	2001.03.30–12.32.53	1.9
915	17	186	122	89	2001.04.13–01.14.53	2.2
916	16	168	187	166	2001.04.06–22.32.15	1.6
918	14	120	154	102	2001.04.08–11.01.30	1.9
919	13	291	156	176	2001.04.09–03.06.22	1.9
927	11	74	128	99	2001.04.02–23.14.28	2.3
930	10	110	61	73	2001.04.08–10.48.59	2.2
938	8	207	52	89	2001.08.05–22.32.57	1.5
940	7	106	99	73	2001.04.08–10.32.47	2.2
941	7	84	76	75	2001.04.09–01.26.02	1.5
942	6	91	165	54	2001.04.08–22.39.32	1.5
951	4	25	60	26	2001.04.02–19.17.33	1.8
968	4	34	90	12	2001.04.10–10.10.00	2.6

Note: x, y and z indicate the dimensions of the box that contains the events of the corresponding multiplet along the E–W direction, the N–S direction and depth, respectively.

6 SYNTHETIC TESTS

To test the precision of the relocation results, particularly the presence of distortions induced by the network configuration, we conducted various synthetic tests assuming direct rays in a homogeneous half-space. For this purpose, from one original synthetic multiplet, 300 simulations are generated by perturbing the hypocentres with Gaussian noise. Travel-time differences are calculated and the simulated multiplet earthquakes are then relocated. Two such tests using four stations but different configurations (DIM, TEM, TRI and AIO or PSA) were conducted using *P*- and *S*-wave travel-time delays. The effect of station AIO is particularly interesting since it is the closest station located above the swarm. The first test, which included station AIO, demonstrates that the multiplet geometry is

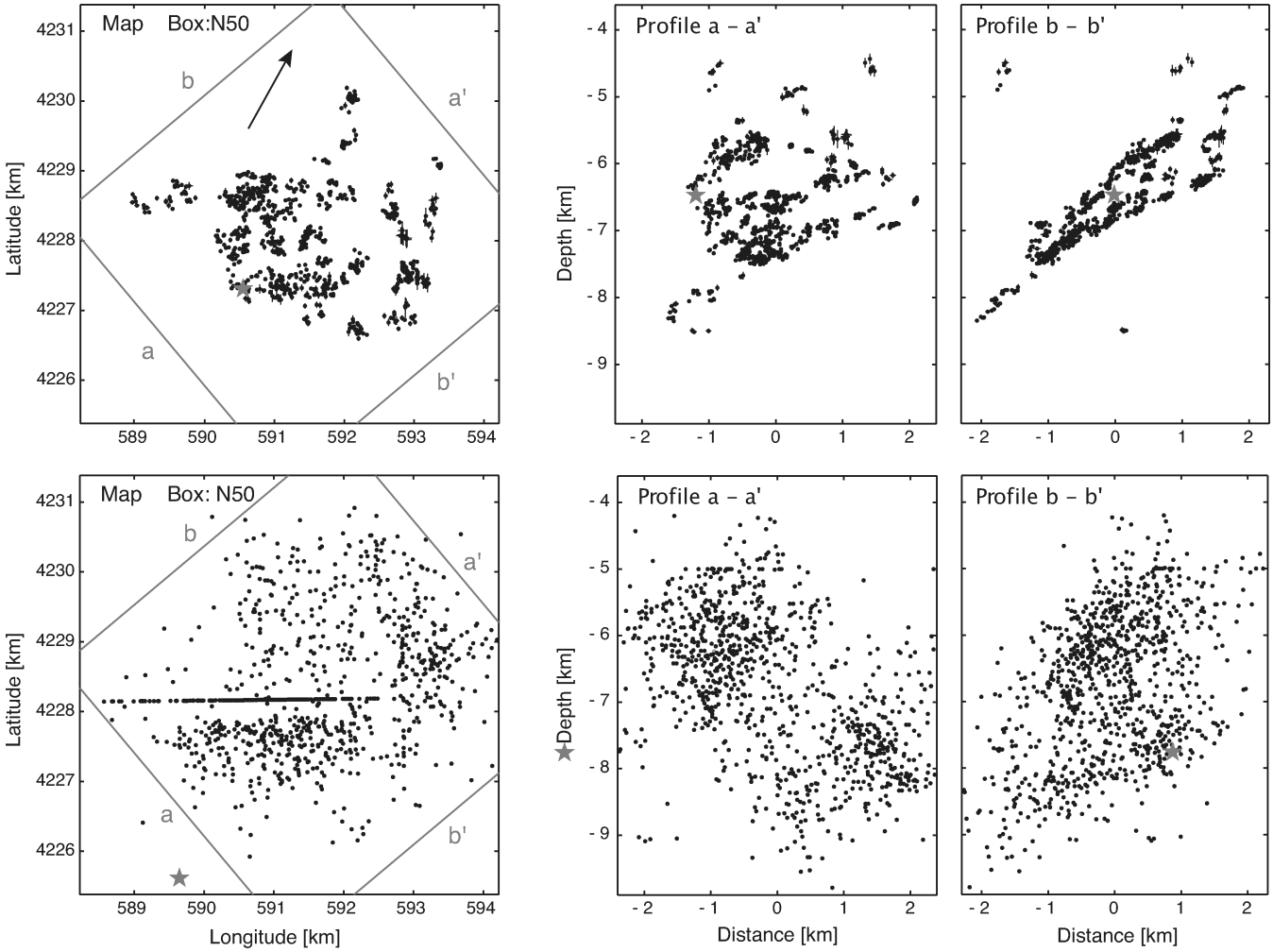

Figure 5. Hypocentres of the 2001 Agios Ioanis earthquake swarm (965 earthquakes) before (bottom row) and after (top row) relocation. (Left panels) Epicentre maps. The grey star represents the Agios Ioanis earthquake (outside the graph for profile a–a') and the arrow shows the slip direction from the focal mechanism of this earthquake. Boxes indicate directions of the orthogonal profiles a–a', oriented 50°N (centre panels), and b–b', oriented 140°N (right panels). Error bars of the relocated seismicity are estimated via Monte-Carlo simulations and correspond to the lower bound of the relocation error.

not distorted and that four stations suffice to achieve reliable results. For the second test, the same stations were used except AIO, which is replaced by PSA. The result clearly shows a geometrical distortion of the simulated multiplets (Fig. 6) and thus suggests that four stations without AIO are not enough to guarantee a reliable relocation.

However, tests on real data, using all available stations, show that the influence of AIO is less important than suggested by the above synthetic tests. To demonstrate this, we located earthquakes of several multiplets while neglecting the AIO recordings and relocated them with Got's method. Although the relocated hypocentres move, as expected, the overall geometry of the multiplet is not significantly different. This is illustrated by two examples (Fig. 7a). This is most probably due to the fact that the distortion is mainly a uniform shift, thus does not significantly alter the multiplet geometry. A similar test is conducted to assess the stability of the reference earthquake relocation using HypoDD. If AIO data is not used at all for the location and relocation, the result is significantly distorted. Nevertheless, this does not reflect the actual situation where only a few reference earthquakes have not been recorded by AIO. We therefore neglected the AIO recordings for only three reference

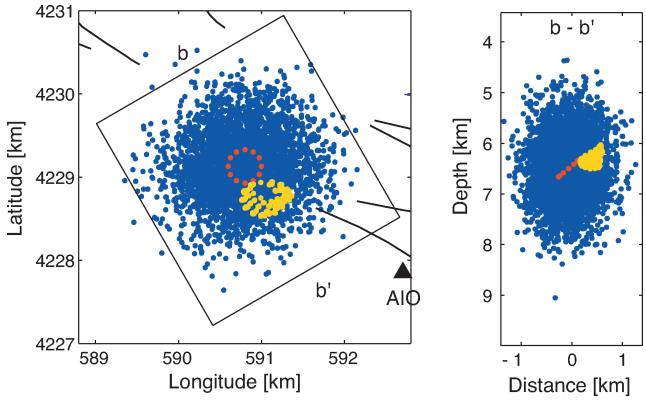

Figure 6. Relocation of 300 Monte-Carlo simulations of a synthetic multiplet calculated in a homogeneous half-space conducted using four stations: DIM, TEM, TRI and PSA. The epicentre map (left) illustrates the original multiplet composed of 12 earthquakes in red, the 300 simulations perturbed by Gaussian noise in blue, and the relocated simulations in yellow. The sides of the boxes indicate the direction of the orthogonal profiles. Profile b–b' (right panel) is oriented 140°N.

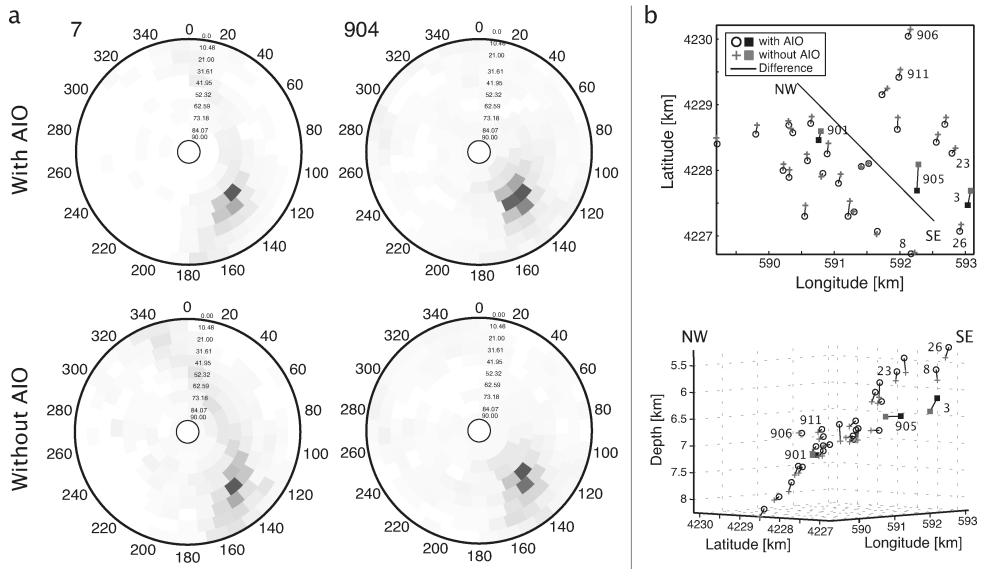

Figure 7. (a) Lower half-sphere stereographic projection representing the pole density distribution for two multiplets (7 and 904). The top row shows the pole densities obtained for multiplets whose events are located and relocated using the seismograms recorded by station AIO, whereas the bottom row shows results obtained without using AIO data. (b) Results of two reference earthquake relocations. The epicentral map is shown on top and a NW-SE profile is shown on the bottom. Black circles show hypocentres relocated while considering reference earthquakes of multiplets 3, 901 and 905 located with AIO data (black squares) and grey crosses illustrate the relocation result obtained considering the reference events of the same three multiplets as above located without AIO data (grey squares).

events (3, 901 and 905) and located them. Thereafter, all reference earthquakes were relocated together with HypoDD (Fig. 7b). The results of the relocation conducted without AIO data for the three events are not significantly different from those obtained using the AIO recordings (Fig. 7b). The mean effect of the absence of AIO data on the hypocentres is a shift towards greater depths and to the north; the mean translation is 132 m in depth and 105 m in latitude. This effect is larger than the relocation error that is $<$50 m, but it is much smaller than the kilometre-scale distortion obtained when the AIO recordings are neglected for all reference earthquakes. Moreover, the reference earthquake 901, which is surrounded by events recorded by station AIO, is shifted in comparable fashion to its neighbors, but also reference earthquake 3, which is not surrounded by earthquakes recorded by AIO, shifts similarly to its neighbors. This shows that no significant distortions are induced by the lack of AIO recordings for a few earthquakes. It is also important to point out that the effect, if any, of the relocation on the reference earthquakes for which AIO recordings are not available (8, 23, 26, 906 and 911) is a shift towards the surface. These facts indicate that the absence of AIO data for a few earthquakes and the possible distortion of the relocation image is corrected, at least in part, by the relocation.

7 SEISMICALLY ACTIVE ZONE

We obtained a reliable geometry for 24 multiplets out of the 27 studied and for 21 submultiplets out of 23. Because of the presence of multiple maxima in the pole density distributions, five multiplets were neglected. Comparison of the nodal planes with the corresponding multiplets' associated planes confirmed 28 multiplet and submultiplet geometries. The determined active fault planes are illustrated in Fig. 8. The majority of these planes are subparallel to the rupture plane of the Agios Ioanis earthquake (220°N/40°NW). The rest are either parallel to the conjugate plane of the greatest earthquake (114°N/77°SW) or dip to the west (e.g. multiplets 908 and 906, respectively; Fig. 8). None of the planes dipping west are conjugate planes of the other above-mentioned planes, regardless of the slip direction. Despite the variety of focal mechanisms, all are consistent with the regional stress regime.

An image of the active structures at depth is constructed by plotting the multiplets on 3-D graphs (Fig. 9). Each ellipse represents the size and location of one multiplet. Its strike and dip are those of the associated plane. The spatial distribution of the multiplets in the earthquake swarm is bimodal. The group of planes situated to the NW of the Agios Ioanis earthquake have a similar geometry and we consider them coplanar based on the relocation uncertainties given by HypoDD ($<$50 m). It is unclear whether the rupture plane of the Agios Ioanis earthquake is part of this group or not. In contrast, the group of planes situated to the NE at shallower depths show similar geometries but are not coplanar. Comparing the vertical offsets to the errors, the relocation indicates active parallel planes. We propose at least three planes represented by (1) multiplet 2, (2) the Agios Ioanis rupture plane and (3) the group of multiplets (907, 910, 904 and 905) situated below the Agios Ioanis rupture plane (Figs 9b and c).

7.1 The Kerinitis Fault

The mean orientation of the active fault planes is 228°N/40°NW, when considering only the multiplets whose orientation is subparallel to the Agios Ioanis earthquake (823 earthquakes, 28 per cent of the swarm). If we assume that the earthquake swarm is represented by a single fault and extend the mean plane to the surface, the trace of the fault is located in the Kerinitis Valley (Fig. 10). The southeastern flank of the valley is a regular NW dipping slope striking 230°N with a dip, measured over 800 m in elevation, equal to 37°. Considering the elevation above sea level, the dip of the plane passing through the fault trace and the reference earthquake of multiplet 1 is 42°. These values agree with the orientation of the Agios Ioanis earthquake rupture plane (220°N/40°NW) and with the mean orientation of the

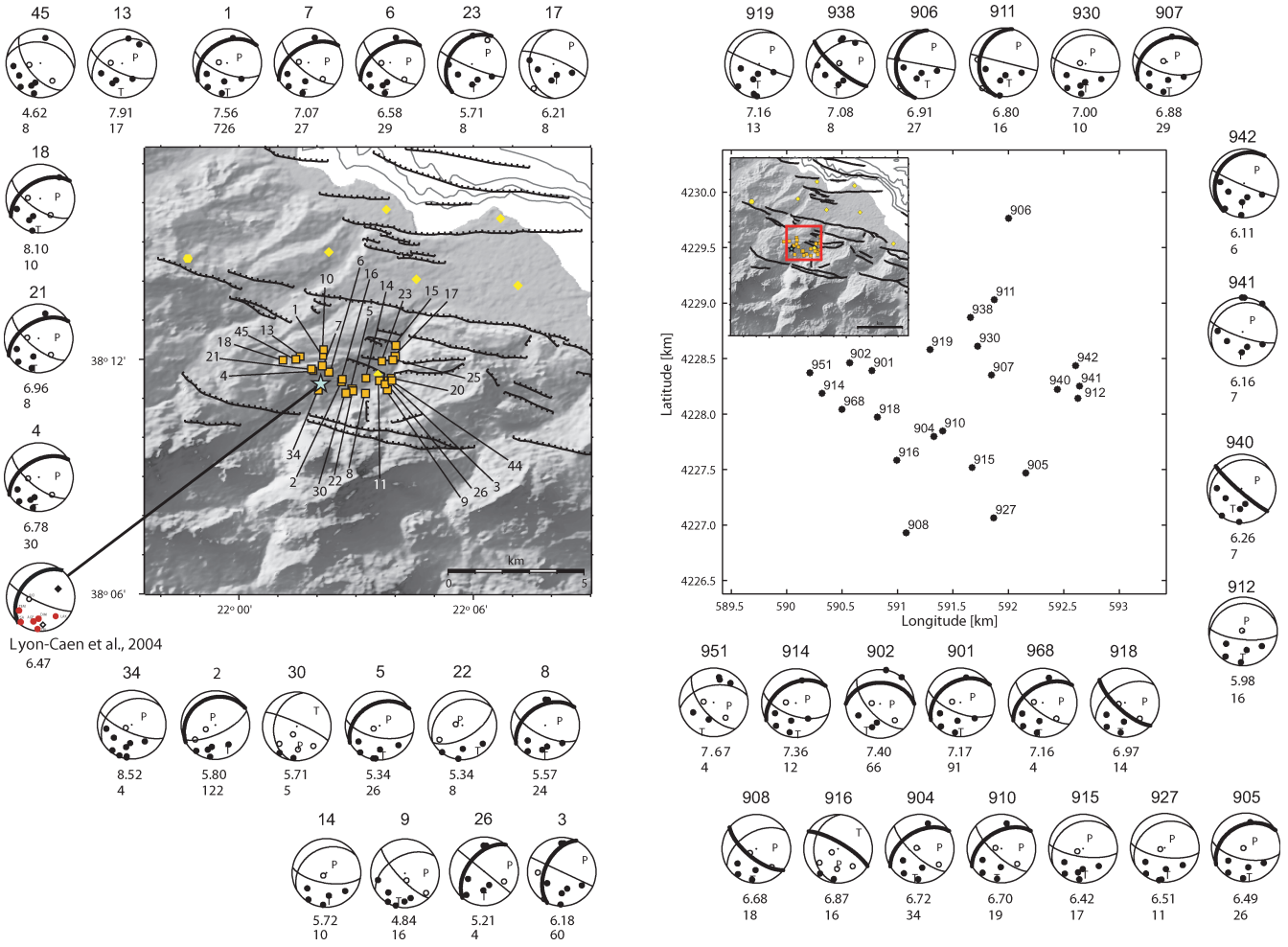

Figure 8. Epicentre map of the multiplet (left panel) and submultiplet (right panel) reference earthquakes and the corresponding representative focal mechanisms illustrating the determined active associated planes (bold nodal planes). The first row of numbers under each mechanism indicates the depth of the reference earthquake and the second, the number of earthquakes in the multiplet.

active structure at depth (228°N/40°NW). Taking into account the topography, the trace becomes curvilinear: on the northern end it follows the valley bottom and on the southern end it coincides with the crest and summit of a mountain. However, assuming that the mountain flank is the fault scarp, the fault trace is more likely to follow the valley bottom (Personal communication M. Ford, 2009). Although the fault is not exposed in the Kerinitis River Valley, Ghisetti *et al.* (2001) and Ford *et al.* (2007) also suggest the presence of a SW–NE oriented transverse fault along the Kerinitis Valley bottom. Ford *et al.* (2007) deduce the presence of a fault based on stratigraphic and structural arguments, by comparing the geometry of Gilbert-type fan deltas located east and west of the valley. These consistent facts argue in favor of the existence of a transverse fault, the Kerinitis Fault.

From a mechanical point of view, this fault was most probably generated as a breached relay ramp connecting the *en échelon* Pirgaki and Mamoussia faults and served to accommodate differential deformation between contiguous blocks. However, the fault has matured too much to be considered only a relay ramp. Indeed, considering the width of the fault, >7.5 km, it is improbable that its length is limited to the distance separating the endpoints of the two *en échelon* faults, 1.5 km apart, because its dimensions would then be disproportionate. It developed to a transverse fault as the rift grew wider and probably faster (Acocella *et al.* 2005). Its orientation and strong horizontal slip component is consistent with the ongoing differential deformation between the western and eastern parts of the rift (Briole *et al.* 2000; Avallone *et al.* 2004), which needs to be accommodated, for example, by distributed N–S oriented faults.

8 SPATIO-TEMPORAL EVOLUTION OF THE SWARM

The swarm started 12 days before the Agios Ioanis earthquake in the immediate vicinity of its rupture plane. Before and immediately after the Agios Ioanis earthquake, activity was confined to the northeastern quadrant, within a radius of 1.5 km of the Agios Ioanis epicentre that is placed at the origin (Fig. 5, top left panel). The activity subsequently shifted to the edges of this zone, predominantly to the east. To the west and south of the Agios Ioanis earthquake, in the direction opposite to slip, no earthquakes occurred (Fig. 5, top left panel).

A refined study of the spatio-temporal evolution, considering the individual events and their origin time, provides evidence of a migration of the seismic activity along the active structure. In this analysis, a simplified geometry is used. We assume that all the seismic activity occurred on a single fault plane coinciding with that of the Agios Ioanis earthquake. The entire relocated earthquake swarm is then rotated in 3-D according to two sets of Euler angles:

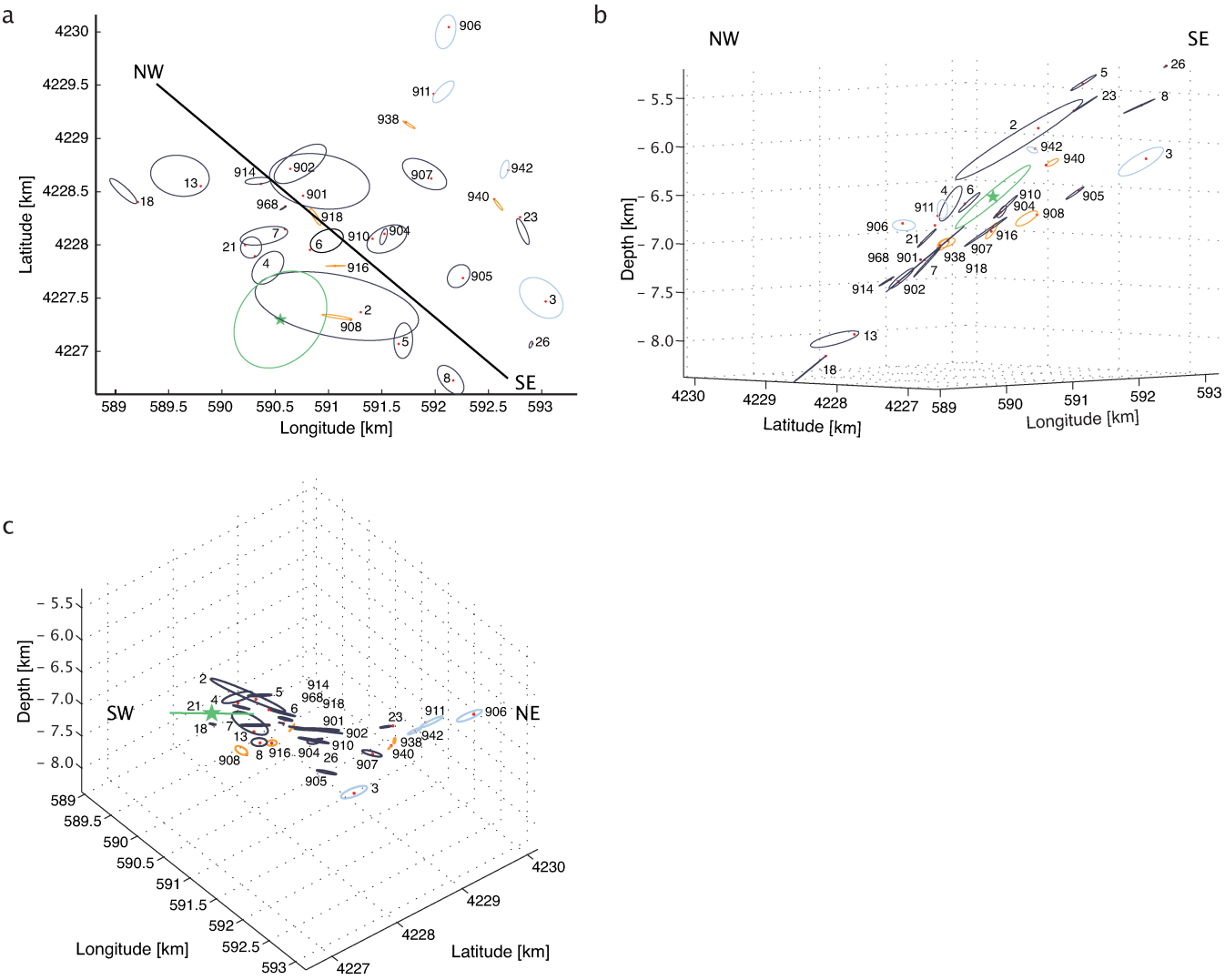

Figure 9. Confirmed active fault planes illustrated by ellipses representative of the multiplets' size and orientation. (a) Map of multiplets, (b) NW–SE profile and (c) view from above at a 40° angle from the horizontal, into the fault plane. Dark blue ellipses illustrate multiplets whose geometry is similar to that of the Agios Ioanis earthquake active fault plane. Orange ellipses depict those whose geometry is similar to that of the conjugate plane of the Agios Ioanis earthquake. Light blue ellipses illustrate multiplets whose geometry show a dip to the west. The green star and ellipse represent the Agios Ioanis epicentre and estimated rupture surface.

(1) 220°/40°/−150° and (2) 220°/40°/−90°. This operation rotates the swarm to a horizontal plane, parallel to the surface. As a result, an image of the swarm from above is obtained in which the inter-event distances are preserved. Two cases are considered, in the first, the slip direction is placed on the *y*-axis, and in the second, the strike direction is placed on the *x*-axis. These are illustrated in Figs 11(a) and (b). The only difference between the two representations is the orientation of the fault strike and slip direction in the horizontal plane (the rotated fault plane). By plotting the distances along the coordinate axes with respect to time, an earthquake migration, perpendicular to the slip direction, towards the surface, is clearly observed (Fig. 11c). Single events do not migrate in sequence, but there is a seismically active patch of constant size, as is suggested by the dashed lines in Figs 11(c) and (f). The approximate speed of migration is 20 m day^{-1}, measured over a distance of 2 km and a period of 100 days. The magnitude and direction of the resultant migration velocity remain unchanged regardless of the orientation of the swarm in the horizontal plane (variation of the third Euler angle; Figs 11d and f). This is an estimate of the true speed of migration because it is measured on the fault plane and not via projection on the Earth's surface.

9 DISCUSSION

The analysis of the spatio-temporal evolution of the Agios Ioanis swarm shows that the earthquakes migrated along the active fault zone. Several reasons could explain such a phenomena, such as stress variations or fluid circulation at depth. Because the migration is directed perpendicular to the slip, towards the surface, and because no earthquake occurs to the southwest of the activated area, we prefer a hypothesis that involves fluids. Pressurized, fluids move along negative pressure gradients, which are reasonably assumed to be directed towards the surface. In the Aigion borehole (AIG10; Fig. 1), Cornet *et al.* (2004) observe over-pressurized fluids (0.9 MPa above hydrostatic) and suspect their presence also at greater depths. From body-wave tomography, Latorre *et al.* (2005) recognized high V_p/V_s ratios between 7 and 9 km depth, under

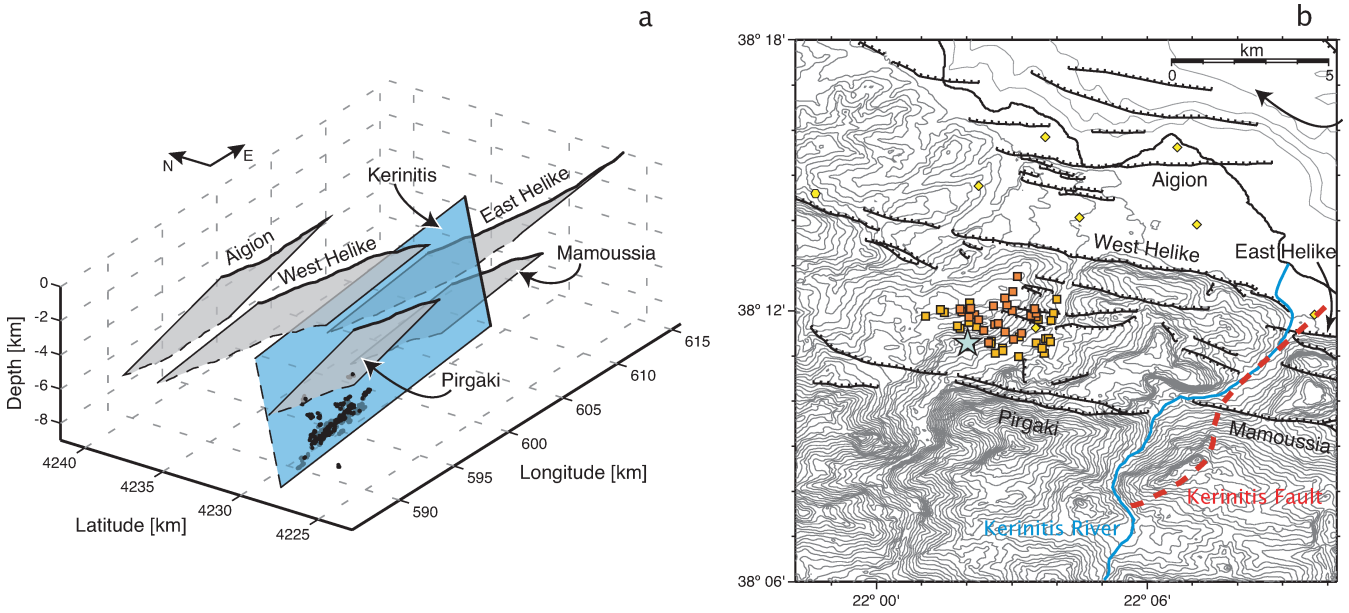

Figure 10. (a) Schema of the major north-dipping normal faults of the southern flank of the Corinth Rift (grey surfaces). The suggested Kerinitis Fault is in blue. The black bold lines indicate the surface trace of the faults and the black dots the relocated swarm earthquakes (grey dots are behind the fault); (b) elevation contour map of the south coast of the western Corinth Gulf within the study area. Contours are drawn every 50 m. Multiplets are in orange and the Agios Ioanis earthquake is in light blue. The Kerinitis Valley bottom is highlighted by its river (blue line) and the estimated Kerinitis Fault trace is illustrated by the red dashed line.

the rift, indicating fluid-saturated rock. Moreover, the implication of fluids is consistent with the idea that the large-scale dynamics of earthquake swarms, in which multiplets are observed, is governed by fluid-induced creep (Bourouis & Bernard 2007). The migration of earthquakes can therefore be thought to reflect fluid paths in the rock.

Earthquake activity associated with fluid flow and corresponding pore-pressure perturbations is typically modeled using the pore-pressure diffusion equation. Applied to induced seismicity, assuming a homogeneous isotropic medium, Shapiro *et al.* (1997) show that the distance from the point source of fluid infiltration to the hypocentres (the radius) is equal to $\sqrt{4\pi Dt}$, where D is the hydraulic diffusion and t is the time relative to the beginning of the process. The application of this model to natural earthquake data is not straightforward for two main reasons. First of all, with natural data, unlike in borehole pumping tests, we do not know the location of the fluid source nor its geometrical aspect. Secondly, to distinguish the dependence of the radius on $\sqrt{t}$, earthquakes must occur at an early stage of the pore-pressure diffusion or during a sufficiently long period. In practice, unless the $\sqrt{t}$ dependence is evident, there is a trade-off between the diffusivity and the time interval that separates the beginning of the fluid diffusion and the triggered earthquakes.

Application to the Agios Ioanis swarm suggests that the fluids did not leak from the deepest point of the fault, but rather from somewhere near the early events of the swarm. Following a forward-modeling approach, the radius shows a $\sqrt{t}$ dependency when measured from points in the area extending south from multiplet 7 to the Agios Ioanis epicentre (Fig. 9a). This area most probably coincides with a relatively highly fractured region that links the single plane at the deepest end of the swarm with the parallel planes at the shallowest end (Fig. 9b). In Fig. 12, we show diffusion curves calculated using our preferred source location, multiplet 21.

Concerning the temporal evolution of the diffusion process, various models are possible based on the data (Fig. 12). However, only the models represented by the solid and the dotted lines in Fig. 12 are relevant. The reason for this is that the earthquake migration velocity deduced by linear approximation from these models must be similar to the one observed in the spatio-temporal analysis, since the underlying phenomena is the same and the earthquakes migrate in a predominant direction. The retained models are quite similar and indicate that the swarm started after a delay of several tens of days relative to the beginning of the fluid infiltration and that the fluids diffused into the rock at about 0.1 $m^2 s^{-1}$. This value compares well to measurements from different settings (e.g. Talwani *et al.* 1991; Shapiro *et al.* 1997, 1999). The reasonably good agreement between the data and the models supports the involvement of fluids in the evolution of the swarm.

First-order approximations of hydraulic conductivity and of rock permeability can be computed by assuming that earthquake migration reflects the propagation of a pressure pulse in the host rock (Shapiro *et al.* 1997; Miller *et al.* 2004). Setting the propagation speed of the pulse equal to the migration rate of the seismic activity, we can express the permeability, k, as a function of the migration velocity, V_m

$$k = \frac{K_H \eta}{\gamma} \approx \frac{V_m \phi \eta}{\gamma}, \quad (1)$$

where K_H is the hydraulic conductivity, η is the viscosity of the pore fluid (water), γ is the specific weight difference between rock and pore fluid (water) and ϕ is the porosity (Miller *et al.* 2004). Applied to our data, we find a hydraulic conductivity equal to 1.2×10^{-5} m s^{-1}, when using 2.3×10^{-4} m s^{-1} for the migration velocity and 0.05 for the porosity (Sulem *et al.* 2004; Géraud *et al.* 2006). The obtained value is similar to the one for the Corinth Rift Pindos limestone measured by Cornet *et al.* (2004) (Table 2) and is comparable to the one obtained for the fractures in borehole EQ1 (Rettenmaier *et al.* 2002; Giurgea *et al.* 2004), which is situated just north of the earthquake swarm (Fig. 1). In addition, by setting $\gamma = 0.017$ MPa/m and $\eta = 10^{-3}$ Pas, we obtain a rock permeability

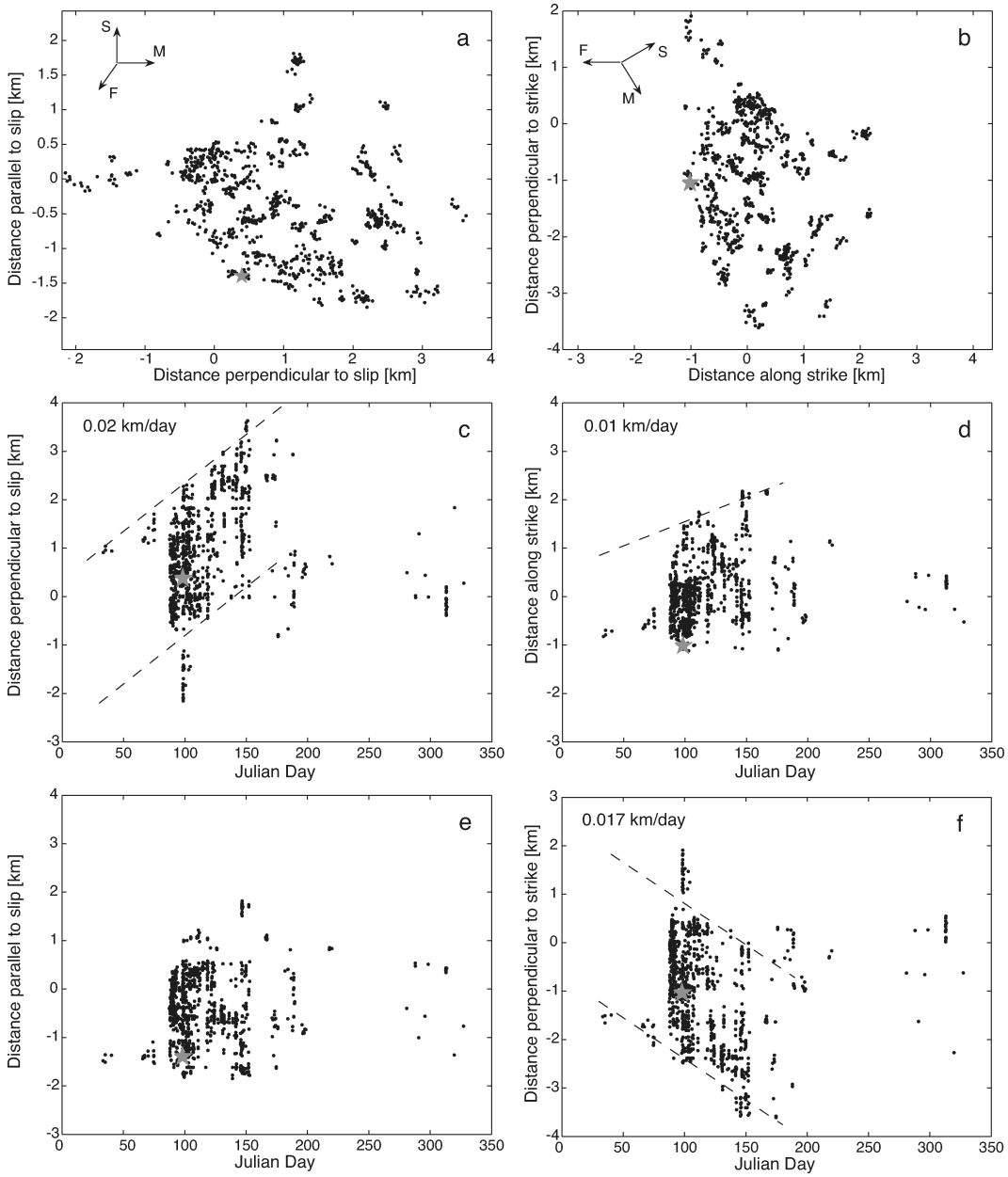

Figure 11. Epicentre maps of the swarm earthquakes after rotation by the Euler angles: 220°/40°/− 150° (a) and 220°/40°/− 90° (b). The grey star represents the Agios Ioanis earthquake. The arrows indicate the direction of slip, S, fault strike, F and earthquake migration, M. (c) Distance perpendicular to slip as a function of time. (d) Distance along strike as a function of time. (e) Distance parallel to slip as a function of time. (f) Distance perpendicular to strike as a function of time. The graphs show a natural earthquake migration directed towards the surface migrating at about 20 m day^{-1}.

equal to 7×10^{-13} m^2. This compares with the value (10^{-13} m^2) inferred by Géraud *et al.* (2006) for the Pirgaki Fault core. Although the permeability is smaller than that measured in other regions of active deformation (e.g. Miller *et al.* 2004), it is higher than the value measured for undamaged limestone in our study area or that generally assumed for a stable crust (Table 2). Thus, it appears to be a reasonable estimate, consistent with the rapid N–S extension occurring in the Corinth Rift.

10 CONCLUSION

Thanks to increased resolution of the seismicity image gained by earthquake relocation, we have mapped and characterized the active faults at depth responsible for the unusual 2001 Agios Ioanis earthquake swarm in the western Corinth Rift. The geometrical analysis of the seismically active zone reveals a complex structure involving several, simultaneously active, parallel planes. This study confirms the existence of the hitherto unexposed Kerinitis Fault, a dextral oblique-slip normal fault that strikes 230°N and dips at 40°NW. Its orientation is in agreement with the focal mechanism of the largest earthquake of the swarm and with the regional extensional stress regime. The orientation and large strike-slip component indicated by the focal mechanism of the $M_w = 4.3$ Agios Ioanis earthquake suggest that this transverse fault may play a role in the accommodation of the differential deformation between the western and eastern parts of the rift. The spatio-temporal study of the earthquake swarm shows a clear natural earthquake migration that

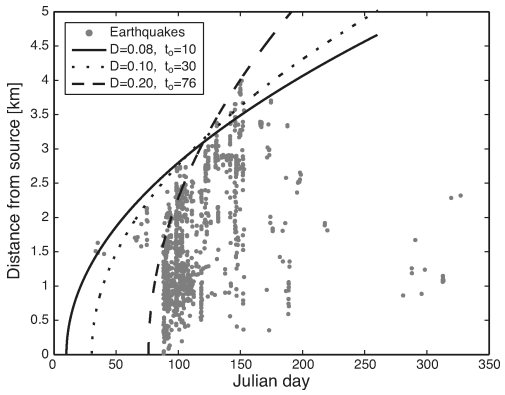

Figure 12. Pore-pressure diffusion phenomena represented by the distance from fluid source (multiplet 21, see text for explanation) to hypocentres as a function of time. Earthquakes are represented by the grey points and the curves illustrate different models of pore-pressure diffusion: $r = \sqrt{4\pi Dt}$. Hydraulic diffusion (D) units are $m^2\,s^{-1}$ and t_o is the origin time of the diffusion in days.

Table 2. Values of hydraulic conductivity, K_H, and permeability, k, obtained in this study compared to those obtained by other studies.

	Region	Study
K_H (ms^{-1})		
1.2×10^{-5}	Corinth	This study
1.1×10^{-5} to 1.5×10^{-5}	Corinth	Cornet *et al.* (2004)
1×10^{-6}	Corinth	Giurgea *et al.* (2004)
k (m^2)		
7×10^{-13}	Corinth	This study
1×10^{-13}	Corinth	Géraud *et al.* (2006)
4×10^{-11}	Colfiorito (IT)	Miller *et al.* (2004)
10^{-16} to 10^{-18}	Stable Crust	Manning (1999)

evolved perpendicular to the slip direction, towards the surface, at a speed of 20 m day^{-1}. Good agreement between the data and the pore-pressure diffusion model strongly suggests the involvement of fluids in the spatio-temporal evolution of the Agios Ioanis swarm. We estimate the hydraulic conductivity and the permeability of the host rock to be 1.2×10^{-5} m s^{-1} and 7×10^{-13} m^2, respectively. Fluid circulation at depth and the relatively high permeability indicate a fractured medium and attest the complexity and heterogeneity of the western Corinth Rift, a fact corroborated by the complex structure of the seismically active zone analyzed, the heterogeneous orientations of the fault planes, and the high b-values.

ACKNOWLEDGMENTS

This study was supported by the European projects AEGIS, contract: IST-2000-26450, coordinated by F. Cornet, and 3HAZ, contract: 004043 (GOCE)-3HAZ-Corinth, coordinated by P. Bernard. We thank A. Deschamps and G. Patau for the preliminary data processing, J.L. Got for giving us full access to his relocation computer codes, P. Bernard for useful discussions on this unusual earthquake swarm. Authors particularly thank M. Ford for discussions on geological aspects of the western Corinth Rift as well as for reading and commenting our paper. Authors also thank M. Cocco, J.-L. Got, and an anonymous reviewer for their helpful comments and constructive reviews.

REFERENCES

Acocella, V., Morvillo, P. & Funiciello, R., 2005. What controls relay ramps and transfer faults within rift zones? Insight from analogue models, *J. Struct. Geol.,* **27**(3), 397–408.

Antonioli, A., Piccinini, D., Chiaraluce, L. & Cocco, M., 2005. Fluid flow and seismicity pattern: evidence from the Umbria-Marche (central Italy) seismic sequence, *Geophys. Res. Lett.,* **32,** L10311, doi:10.1029/2004GL022256.

Armijo, R., Meyer, B., King, G.C.P., Rigo, A. & Papanastassiou, D., 1996. Quaternary evolution of the Corinth Rift and its implications for the Late Cenozoic evolution of the Aegean, *Geophys. J. Int.,* **126,** 11–53.

Avallone, A. *et al.*, 2004. Analysis of eleven years of deformation measured by GPS in the Corinth Rift Laboratory area, *C. R. Geosci.,* **336,** 301–311.

Bernard, P. *et al.*, 1997. The Ms = 6.2, June 15, 1995 aigion earthquake (Greece): evidence for low angle normal faulting in the Corinth Rift, *J. Seismol.,* **1,** 131–150.

Bernard, P. *et al.*, 2006. Seismicity, deformation and seismic hazard in the western rift of Corinth: new insights from the Corinth Rift Laboratory (CRL), *Tectonophysics,* **426**(1–2), 7–30.

Bourouis, S. & Bernard, P., 2007. Evidence for coupled seismic and aseismic fault slip during water injection in the geothermal site of Soultz (France) and implications for seismogenic transients, *Geophys. J. Int.,* **169**(2), 723–732.

Bourouis, S. & Cornet, F.H., 2009. Microseismic activity and fluid fault interactions: some results from the Corinth Rift Laboratory (CRL), Greece, *Geophys. J. Int.*, **178**(1), 561–580.

Briole, P. *et al.*, 2000. Active deformation of the Corinth Rift, Greece: results from repeated Global Positioning System surveys between 1990 and 1995, *J. geophys. Res.,* **105**(B11), 25605–25625.

Brooks, M. & Ferentinos, G., 1984. Tectonics and sedimentation in the Gulf of Corinth and the Zakynthos and Kefallinia channels, western Greece, *Tectonophysics,* **101,** 25–54.

Chiaraluce, L. *et al.*, 2004. Complex normal faulting in the Apennines thrust-and-fold belt: the 1997 seismic sequence in central Italy, *Bull. seism. Soc. Am.,* **94**(1), 99–116.

Console, R. & Di Giovambattista, R., 1987. Local earthquake relative location by digital records, *Phys. Earth planet. Inter.,* **47,** 43–49.

Cornet, F.H., Doan, M.L., Moretti, I. & Borm, G., 2004. Drilling through the active Aigion Fault: the AIG10 well observatory, *C. R. Geosci.,* **336,** 395–406.

Fehler, M., House, L. & Kaieda, H., 1987. Determining planes along which earthquakes occur: method and application to earthquakes accompanying hydraulic fracturing, *J. geophys. Res.,* **92**(B9), 9407–9414.

Flotté, N., 2003. Caractérisation structurale et cinématique d'un rift sur détachement: Le Rift de Corinthe-Patras, Grèce, *PhD thesis*, Université Paris-Sud.

Ford, M., Williams, E.A., Malartre, F. & Popescu, S.M., 2007. Stratigraphic architecture, sedimentology and structure of the Vouraikos Gilbert-type fan delta, Gulf of Corinth, Greece, in *Special Publication of the International Association of Sedimentologists,* Vol. 83, pp. 49–90, eds Nichols, G.J., Williams, E.A. & Paola, C., Blackwell Publishing, Oxford.

Frechet, J., 1985. Sismogenèse et doublets sismiques, *PhD thesis*, Université Scientifique et Médicale de Grenoble.

Fryer, R.J., 1975. On the subdivision of a spherical surface into elements of equal area, *Geophys. J. R. astr. Soc.,* **42,** 883–891.

Géraud, Y., Diraison, M. & Orellana, N., 2006. Fault zone geometry of a mature active normal fault: a potential high permeability channel (Pirgaki fault, Corinth rift, Greece), *Tectonophysics,* **426**(1–2), 61–76.

Ghisetti, F.C., Vezzani, L., Agosta, F., Sibson, R. & Moretti, I., 2001. Tectonic setting and sedimentary evolution of the south-west margin of the Corinth Rift (Aigion-Xylocastro area), Technical Report 56 207, Institut Fran cais du Pétrole.

Giurgea, V., Rettenmaier, D., Pizzino, L., Unkel, I., Hötzl, H., Förster, A. & Quattrocchi, F., 2004. Preliminary hydrogeological interpretation of the Aigion area form the AIG10 borehole data, *C. R. Geosci.,* **336,** 467–475.

Got, J.L., Frechet, J. & Klein, F., 1994. Deep fault plane geometry inferred from multiplet relative relocation beneath the south flank of Kilauea, *J. geophys. Res.,* **99,** 15375–15386.

Hainzl, S., 2004. Seismicity patterns of earthquake swarms due to fluid intrusion and stress triggering, *Geophys. J. Int.,* **159,** 1090–1096.

Jenatton, L., Guiguet, R., Thouvenot, F. & Daix, N., 2007. The 16,000-event 2003-2004 earthquake swarm in Ubaye (French Alps), *J. geophys. Res.,* **112,** B11304, doi:10.1029/2006JB004878.

King, G.C.P. *et al.*, 1985. The evolution of the Gulf of Corinth (Greece): an aftershock study of the 1981 earthquakes, *Geophys. J. R. astr. Soc.,* **80,** 677–683.

Lambotte, S., Lyon-Caen, H., Bernard, P., Pacchiani, F. & Bourouis, S., 2007. Multiplet identification from a large earthquake database in the western part of the Corinth Gulf, in preparation.

Latorre, D., Virieux, J., Monfret, T., Monteiller, V., Vanorio, T., Got, J.L. & Lyon-Caen, H., 2005. A new seismic tomography of Aigion area (Gulf of Corinth-Greece) from the 1991 dataset, *Geophys. J. Int.,* **159,** 1013–1031.

Lee, W.H.K. & Lahr, J.C., 1972. A computer program for determining hypocenter, magnitude, and first motion pattern of local earthquakes, Open-file report 75-311, U.S. Geological Survey.

Lyon-Caen, H., Papadimitriou, P., Deschamps, A., Bernard, P., Makropoulos, K., Pacchiani, F. & Patau, G., 2004. First results of the CRLN seismic array in the western Corinth Gulf: Evidence for old fault reactivation, *C. R. Geosci.,* **336,** 343–351.

Manning, C.E., 1999. Permeability of the continental crust: Implications of geothermal data and metamorphic systems, *Rev. Geophys.,* **37**(1), 127–150.

McKenzie, D.P., 1972. Active tectonics of the Mediterranean region, *Geophys. J. R. astr. Soc.,* **30,** 109–185.

Micarelli, L., Moretti, I. & Daniel, J.M., 2003. Structural properties of rift-related normal faults: the case of the Gulf of Corinth, Greece, *J. Geodyn.,* **36,** 275–303.

Miller, S.A., Collettini, C., Chiaraluce, L., Cocco, M., Barchi, M. & Kaus, B., 2004. Aftershocks driven by a high-pressure CO_2 source at depth, *Nature,* **427,** 724–727.

Moretti, I., Sakellariou, D., Lykousis, V. & Micarelli, L., 2003. The Gulf of Corinth: and active half graben?, *J. Geodyn.,* **36,** 323–340.

Noir, J., Jacques, E., Békry, S., Adler, P.M., Tapponnier, P. & King, G.C.P., 1997. Fluid flow triggered migration of events in the 1989 Dobi earthquake sequence of central afar, *Geophys. Res. Lett.,* **24**(18), 2335–2338.

Oppenheim, A.V. & Schafer, R.W., 1975. *Digital Signal Processing,* Prentice Hall, Englewood Cliffs, New Jersey.

Pacchiani, F., 2006. Etude sismologique des failles noramles actives du Rift de Corinthe, *PhD thesis*, Université Paris XI.

Phillips, W.S., Rutledge, J.T., House, L.S. & Fehler, M.C., 2002. Induced microearthquake patterns in hydrocarbon and geothermal reservoirs: Six case studies, *Pure appl. Geophys.,* **159**(1–3), 345–369.

Poupinet, G., Ellsworth, W.L. & Frechet, J., 1984. Monitoring velocity variations in the crust using earthquake doublets: an application to the Calaveras Fault, California, *J. geophys. Res.,* **89**(B7), 5719–5731.

Rettenmaier, D., Giurgea, V., Hötzl, H., Förster, A. & Nikas, K., 2002. Geological mapping and hydrogeological testing of the block-faulted system in the hinterland of Aigion, Proceedings of the 27th General Assembly of the European Geophysical Society, Nice, France.

Rigo, A., Lyon-Caen, H., Armijo, R., Deschamps, A., Hatzfeld, D., Makropoulos, K., Papadimitriou, P. & Kassaras, I., 1996. A microseismic study in the western part of the Gulf of Corinth (Greece): implications for large-scale normal faulting mechanisms, *Geophys. J. Int.,* **126,** 663–668.

Rubin, A.M. & Gillard, D., 2000. Aftershock asymmetry/rupture directivity among central San Andreas Fault microearthquakes, *J. geophys. Res.,* **105**(B8), 19'095–19'109.

Schaff, D.P., Bokelmann, G.H.R., Beroza, G.C., Waldhauser, F. & Ellsworth, W.L., 2002. High-resolution image of Calaveras Fault seismicity, *J. geophys. Res.,* **107**(B7), 2186, doi:10.1029/2001JB000633.

Scholz, C.H., 2002. *Mechanics of Earthquakes and Faulting,* Cambridge University Press.

Shapiro, S.A., Huenges, E. & Borm, G., 1997. Estimating the crust permeability from fluid-injection-induced seismic emission at the KTB site, *Geophys. J. Int.,* **131,** F15–F18.

Shapiro, S.A., Audigane, P. & Royer, J.J., 1999. Large-scale *in situ* permeability tensor of rocks from induced microseismicity, *Geophys. J. Int.,* **137,** 207–213.

Sulem, J., Vardoulakis, I., Ouffroukh, H., Boulon, M. & Hans, J., 2004. Experimental characterization of the thermo-poro-mechanical properties of the Aegion Fault gouge, *C. R. Geosci.,* **336,** 455–466.

Talwani, P., Cobb, J.S. & Schaeffer, M.F., 1991. In situ measurements of hydraulic properties of a shear zone in northwestern South Carolina, *J. geophys. Res.,* **104**(B7), 14993–15003.

Waldhauser, F. & Ellsworth, W.L., 2000. A double-difference earthquake location algorithm: Method and application to the Northern Hayward Fault, *Bull. seism. Soc. Am.,* **90**(6), 1353–1368.

Waldhauser, F. & Ellsworth, W.L., 2002. Fault structure and mechanics of the Hayward Fault, California, from double-difference earthquake locations, *J. geophys. Res.,* **107**(B3), doi:10.1029/2000JB000084.

Zahradník, J., Janský, J., Sokos, E., Serpetsidaki, A., Lyon-Caen, H. & Papadimitriou, P., 2004. Modeling the $M_L = 4.7$ mainshock of the February-July 2001 earthquake sequence in Aigion, Greece, *J. Seismol.,* **8,** 247–257.